


Article

Hardening of HVOF-Sprayed Austenitic Stainless-Steel Coatings by Gas Nitriding

Thomas Lindner *, Pia Kutschmann, Martin Löbel and Thomas Lampke 

Materials and Surface Engineering Group, Institute of Materials Science and Engineering, Chemnitz University of Technology, D-09107 Chemnitz, Germany; pia.kutschmann@mb.tu-chemnitz.de (P.K.); martin.loebel@mb.tu-chemnitz.de (M.L.); thomas.lampke@mb.tu-chemnitz.de (T.L.)

* Correspondence: th.lindner@mb.tu-chemnitz.de; Tel.: +49-371-531-38287

Received: 24 August 2018; Accepted: 27 September 2018; Published: 29 September 2018



Abstract: Austenitic stainless steel exhibits an excellent corrosion behavior. The relatively poor wear resistance can be improved by surface hardening, whereby thermochemical processes offer an economic option. The successful diffusion enrichment of bulk material requires a decomposition of the passive layer. A gas nitriding of high velocity oxygen fuel spraying (HVOF)-sprayed AISI 316L coatings without an additional activation step was studied with a variation of the process temperature depending on the heat-treatment state of the coating. A successful nitrogen enrichment was found in as-sprayed condition, whereas passivation prevents diffusion after solution heat treatment. The phase composition and microstructure formation were examined. The crystal structure and lattice parameters were determined using X-ray diffraction analysis. The identified phases were assigned to the different microstructural elements using the color etchant Beraha II. In as-sprayed condition, the phase formation in the coating is related to the process temperature. The formation of the S-phase with interstitial solvation of nitrogen is achieved by a process temperature of 420 °C. Precipitation occurs during the heat treatment at 520 °C. In both cases, a significant increase in wear resistance was found. The correlation of the thermochemical process parameters and the microstructural properties contributes to a better understanding of the requirements for the process combination of thermal spraying and diffusion.

Keywords: thermal spraying; thermochemical treatment; nitriding; hardening; S-phase; AISI 316L; stainless steel; high velocity oxygen fuel spraying (HVOF)

1. Introduction

Surface hardening of austenitic stainless steel in bulk material state involves an activation step degrading the passivation layer, which prevents surface diffusion. Depending on the temperature–time profile, the phase formation for carbon or nitrogen enrichment differs. Increasing process temperature and duration can cause the formation of precipitates that reduce the corrosion resistance due to chromium depletion. Low-temperature thermochemical treatment can permit a supersaturation of the crystal matrix by interstitial elements. Carbon and nitrogen can diffuse into the interstices of the face-centred cubic (FCC) lattice after dissolving the passivation layer [1–3]. These heat treatment processes are mainly used in the case of bulk material treatment [4]. Qualifying a process combination of coating technologies and additional surface hardening can be a choice for new applications. The separation of bulk and surface properties enables a multi-material design and a better adaption to local requirements. Furthermore, repair solutions are possible. In particular, thermal spraying offers the possibility to prevent a degradation of the metastable S-phase layer by limitation of heat input.

The fundamental feasibility of combining the processes of thermal spraying for deposition of austenitic stainless-steel coatings and thermochemical treatment has been shown in several studies [4–11]. However, the need of using the special process management of thermochemical treatment with the activation step designed for bulk material is not proven for thermally sprayed coatings. The reactions occurring while processing the austenitic feedstock material as well as the microstructure of thermally sprayed coatings raise doubts on the expediency of the parameter settings for thermochemical treatment.

Nestler et al. investigated the diffusion enrichment of high velocity oxygen fuel spraying (HVOF)-sprayed AISI 316L coatings in a gas nitriding process without an additional activation step. The formation of a compound layer by nitrogen diffusion from the surface into the coating was proven in a temperature range between 500 °C and 580 °C. The intended enrichment of the substrate material through the coating was not achieved. They assumed that a nitrogen transport through the coating structure is suppressed by the effect of low porosity and chemical composition [5]. On the other hand, Park et al. focussed on the plasma nitriding and nitro-carburizing process to improve the wear resistance of AISI 316L coatings by precipitation hardening [6]. After nitriding, the compound layer consists of CrN, Fe₃N and Fe₄N, but the diffusion depth is lower compared to the findings of Nestler et al. [5,6].

Wielage et al. first mentioned a successful S-phase formation for HVOF-sprayed AISI 316L coatings without chromium depletion by low temperature carburization with an additional surface-activation step [7]. Adachi et al. and Lindner et al. investigated further methods of low-temperature thermochemical processes. Adachi et al. carried out several studies on AISI 316L coatings produced by different thermal-spraying processes and a subsequent plasma process to enrich the coating surface with nitrogen, carbon, or both. They found that the diffusion-layer thickness is influenced by the temperature, whereas the coating condition and microstructure do not promote the interstitial diffusion [4,8–10]. Lindner et al. applied a gas nitro-carburizing process on HVOF-sprayed AISI 316L coatings and determined a certain porosity effect on diffusion depth [11]. Both noticed that the low-temperature processes enable the formation of the S-phase at regions near the surface area in thermally sprayed austenitic stainless-steel coatings with a diffusion depth slightly larger or comparable to bulk material. A lattice expansion of the austenitic phase was found by X-ray diffraction due to the interstitial solution of nitrogen and carbon atoms [7,11]. The described structural effects for thermally sprayed coatings are comparable to the results in bulk material state [12,13]. The dependency on the considered crystal planes follows the anisotropic elastic behavior of austenite, whereby enrichment of nitrogen causes a higher distortion than carbon. Both compound-layer formation by precipitation hardening and S-phase formation by interstitial solvation result in a significant improvement of the wear resistance of thermally sprayed stainless-steel coatings [4,5,7–11].

The present study focuses on the hardenability of HVOF-sprayed AISI 316L coatings by thermochemical treatment without an initial surface activation. A gas-nitriding process was performed using different temperature–time profiles aiming at precipitation and solution hardening. The diffusion behavior and phase formation were investigated with regard to the coating's structure. The wear behavior was determined for the untreated and the gas-nitrided states. A solution heat treatment of coatings was performed to reduce deviations in the element concentration caused by thermal-spray processing. The proven change of diffusion behavior permits alternative parameter settings for the thermochemical treatment of thermally sprayed coatings. The results contribute to a better understanding of material behavior in conjunction with the S-phase formation of austenitic stainless-steel coatings.

2. Materials and Methods

As coating material, gas-atomized AISI 316L powder was used in a fraction of $-53+20$ µm. Substrates were prepared out of the same kind of stainless steel using bar material with a diameter of 40 mm in cuts of 8 mm. After grid blasting the front surface using EK-F 24 (3 bar, 20 mm distance,

70° angle), the samples were cleaned for 5 min in an ultrasonic ethanol bath. The thermally sprayed coatings were produced by a HVOF K2 system (GTV, Luckenbach, Germany) with the parameters shown in Table 1. With an average coating thickness of 297 μm after 12 passes, the mean growth rate per pass is approximately 25 μm .

Table 1. The parameters of the HVOF thermal-spraying process with a GTV-K2 system.

| Kerosene Flow Rate (L/h) | Oxygen Flow Rate (L/min) | λ | Combustion Chamber Pressure (bar) | Spraying Distance (mm) | Nozzle (mm) | Transverse Speed (m/s) | Offset (mm) | Powder Feed Rate (g/min) | Gas Feed (Argon) (L/min) | Wiper |
|--------------------------|--------------------------|-----------|-----------------------------------|------------------------|-------------|------------------------|-------------|--------------------------|--------------------------|-------|
| 24 | 900 | 1.1 | 7.1 | 350 | 150/14 | 1 | 5 | 70 | 2 \times 8 | NL |

The average chemical composition of the main alloying elements was analyzed by X-ray fluorescence (XRF) utilizing a FISCHERSCOPE X-RAY XAN (Helmut Fischer, Sindelfingen, Germany) with 30 kW and 1 mm collimator lens for substrate, feedstock and coating material. The evaluation software Fischer XAN-WinFTM 6.33 (Helmut Fischer, Sindelfingen, Germany) was used. Five positions were measured for each sample. Furthermore, a quantification of the oxygen content was carried out using carrier-gas hot extraction (CGHE) TC600 (Leco, St. Joseph, MI, USA).

While it can be expected that the passivation layer prevents a diffusion enrichment of the austenitic stainless-steel bulk sample, additionally a ferritic steel grad AISI 1015 was chosen as further reference. The surface of the coated samples and the bulk material were polished up to mesh 1000. The final coating thickness is approximately 270 μm . A solution heat treatment at 1100 °C for 4 h was performed in a Torvac 12 Mark IV furnace under vacuum (10^{-4} mbar). The bulk references and the coatings in heat-treated and as-sprayed condition were gas nitrided in an industrial vacuum chamber retort WMU heat-treatment furnace using the parameters shown in Table 2. The different treatment temperatures were adapted to the different hardening techniques.

Table 2. Gas-nitriding parameters.

| Process Gas | Volume Flow (L/h) | Temperature (°C) | Duration (h) |
|-----------------|-------------------|------------------|--------------|
| NH ₃ | 1000 | 520; 420 | 36; 30 |

Metallographic cross-sections were prepared according to standard metallographic procedures. After hot mounting the section parts in conductive resin, grinding, and polishing, the samples were etched using Beraha II color etchant to visualize the different microstructural constituents. The distinguished color contrast gives evidence of diffusion enrichment as well as their presence and distribution. The metallographic investigations were performed using an optical microscope GX51 (Olympus, Shinjuku, Japan) equipped with a SC50 camera (Olympus, Shinjuku, Japan).

The microhardness was measured on the cross-section using a FISCHERSCOPE HM2000 XYm (Helmut Fischer, Sindelfingen, Germany) with 0.01 kp. The diffraction studies were performed by X-ray diffraction (XRD) using a D8 DISCOVER diffractometer (Bruker AXS, Billerica, MA, USA). Co-K α radiation was used with a tube voltage of 40 kV, a tube current of 40 mA, polycap optics for beam shaping, a 1 mm pinhole collimator, and a 1D Lynxeye XE detector (Bruker, MA, USA). The diffraction diagrams were measured in the diffraction angle (2θ) range from 20° to 129° with a step size of 0.01°, and 1.5 s/step, which corresponds to 288 s/step due to the use of the 1D detector. The powder diffraction file (PDF) database 2014 was applied for phase identification and the determination of the lattice parameters.

The tribological properties of the coatings were investigated with the reciprocating ball-on-plane test leant on ASTM G 133 [14] as dry couple and the ball-on-disk test leant on ASTM G 99 [15] as a dry sliding system, both with a spherical counterbodies. The test parameters as well as the counterbody material and diameter are shown in Table 3. The wear volumes and depths were determined with the

3D profilometer MikroCAD (LMI, Teltow, Germany). The wear coefficient K was calculated according to Equation (1), with the wear volume V , the sliding distance l and the normal load F .

$$K = \frac{V}{F \cdot l} \quad (1)$$

Table 3. Testing parameters of wear tests.

| Reciprocating Ball-on-Plane Test | | Ball-on-Disk Test | |
|----------------------------------|--------|----------------------------------|--------|
| Normal load | 26 N | Normal load | 20 N |
| Frequency | 40 Hz | Radius | 5 mm |
| Time | 900 s | Speed | 96 RPM |
| Amplitude | 0.5 mm | Cycles | 15916 |
| Ø Al ₂ O ₃ | 10 mm | Ø Al ₂ O ₃ | 6 mm |

3. Results

3.1. Chemical Composition

The XRF measurements confirm a good agreement between the average chemical composition of the feedstock material and the coatings. Due to the coating process, minor reductions of chromium and molybdenum contents occur. Slight deviations can be found in comparison to the bulk sample. A lower nickel content was observed along with a simultaneous increase in iron concentration. The CGHE quantifies an increase in oxygen content for the HVOF coating. This is related to the atmospheric condition during processing the feedstock, as shown in Table 4.

Table 4. Average chemical composition of the AISI 316L samples in different conditions, measured by XRF and CGHE (main alloy elements in relative wt.%, oxygen in absolute wt.%).

| Sample | Feedstock | HVOF Coating | Substrate |
|----------------|-----------|--------------|-----------|
| Fe | 66.2 | 67 | 70 |
| Cr | 16.7 | 16.5 | 16.8 |
| Ni | 12.8 | 12.7 | 10.1 |
| Mo | 2.8 | 2.3 | 1.9 |
| Mn | 1.5 | 1.5 | 1.2 |
| O ₂ | 0.1 | 0.65 | – |

3.2. Microstructure Analyses

The microstructure of the coating is affected by the solution treatment step. Figure 1 shows the difference in microstructure formation in cross-section. In as-sprayed condition, the single spray particles can be clearly distinguished by the contrast of cluster boundaries including some porosity. The contrast indicates possible oxidation of alloy components at the surface of the single particles. By solution heat treatment, segregations were dissolved, whereas porosity remains.

A successful diffusion enrichment without an initial activation step was found for the AISI 316L HVOF coating in as-sprayed condition. Figure 2 shows the cross-section of the coatings in dependence of the used gas-nitriding parameters. The domains in the microstructure can be distinguished depending on the process temperature using Beraha II color etchant. Within the coating, three phase areas were determined, proving a heterogeneous microstructure. The S-phase appears white, while a brown or blue color indicates the initial austenitic phase. In accordance with the results of Nestler et al., a compound layer is formed on top of the coating at 520 °C [5]. This layer possesses an intense reaction with the color etchant causing a deep contrast. Underneath, a thin, white layer can be detected, which can be assigned to the S-phase. Due to the different etching technique, Nestler et al. do not prove this in their research. Several isolated white particles with a high surface distance indicate

a permeability of the coating. Moreover, the compound-layer thickness above 100 μm proves the influence of the coating porosity, as an AISI 1015 bulk reference shows only 20 μm . Furthermore, a compound-layer thickness of 40 μm and 44 μm was described by Rajendran et al. and Subbiah et al. after gas nitriding of AISI 316LN bulk material by using similar process parameters [16,17].

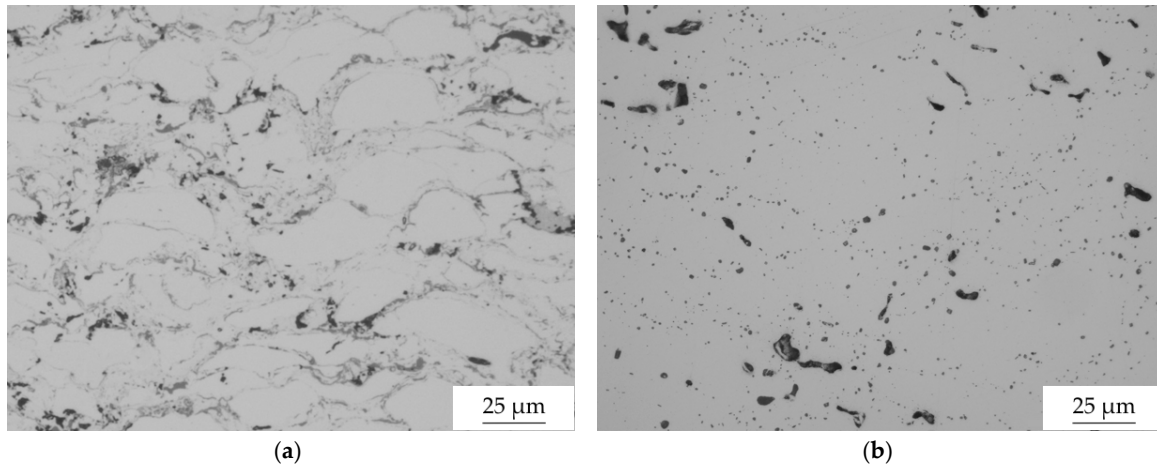


Figure 1. Optical-microscopic images of the AISI 316L HVOF coating in cross-section (a) as-sprayed condition and after (b) solution heat treatment.

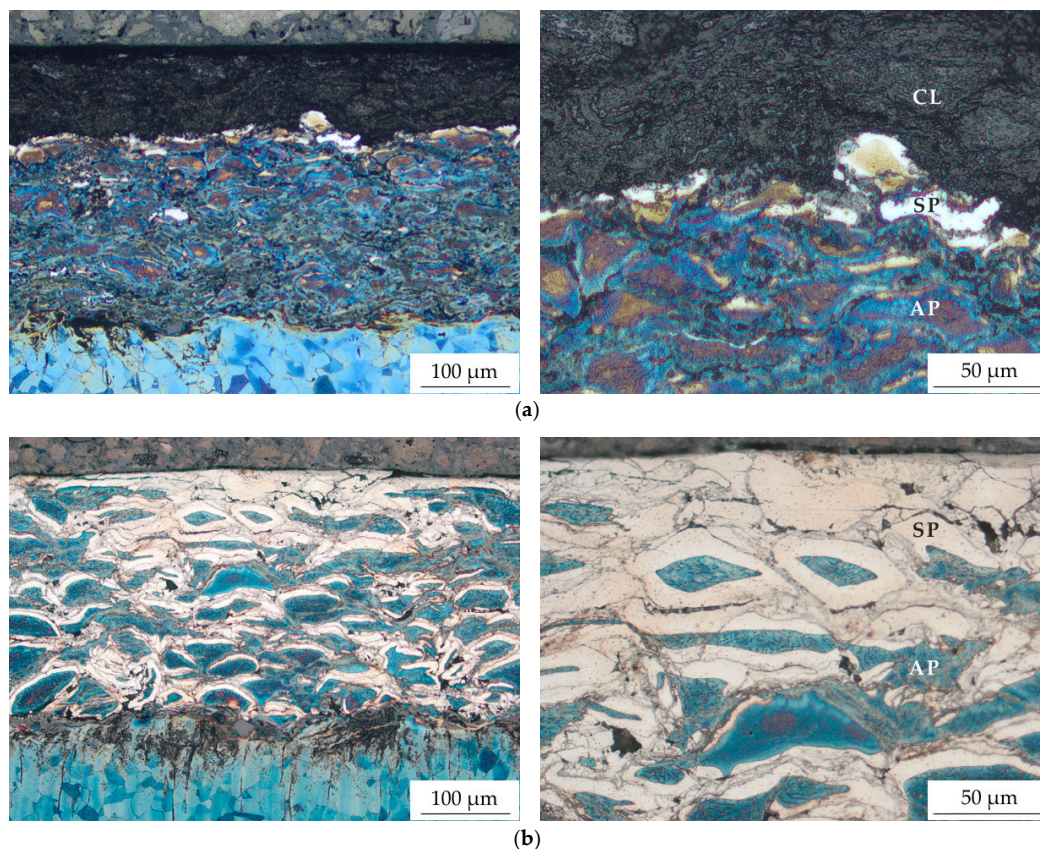


Figure 2. Optical-microscopic images of a Beraha II-etched AISI 316L HVOF coating in as-sprayed conditions after gas nitriding with different parameters (a) gas nitrided, 520 $^{\circ}\text{C}$, 36 h and (b) gas nitrided, 420 $^{\circ}\text{C}$, 30 h in overall view and detail with phase declaration (CL: compound layer; SP: S-phase; AP: austenitic phase).

The reduction of the temperature level and duration of the gas-nitriding process causes a change in phase formation. Precipitates can be avoided, whereas S-phase is formed at the surface of the spray particles, confirming results of gas nitro-carburization [11]. The S-phase can be found between the coating's surface and the coating–substrate interface. The diffusion depth within the single spray particles slightly decreases with increasing distance from the surface, which can be explained by a limitation of exchangeability. Compound-layer formation causes a volume increase that reduces the permeability.

The passive layer was repeatedly mentioned to be an effective diffusion barrier. The results of gas nitriding at 420 °C (Figure 3) prove that no diffusion enrichment can be observed for the bulk material without an activation step. Furthermore, the solution-heat-treated coatings show equal material behavior. No deviation in etchant color occurs, indicating a homogeneous phase distribution. This suggests a homogeneous passivation layer with diffusion protection of the surface. It can be assumed that deviations in element concentrations as well as a heterogeneous oxygen enrichment within the coating are the main reason for the change in diffusion behavior.

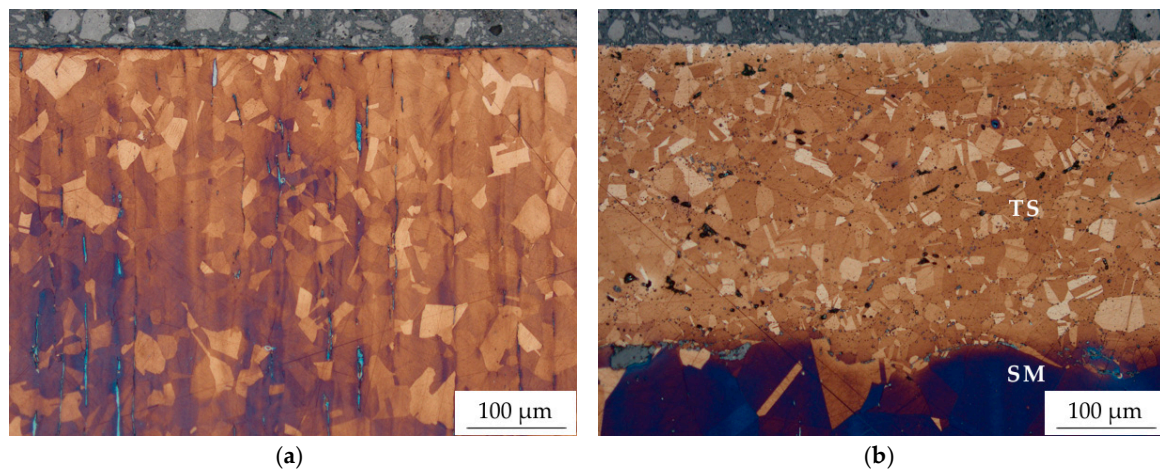


Figure 3. Optical-microscopic images of a Beraha II-etched bulk sample and the solution-heat-treated AISI 316L HVOF coating after gas nitriding 420 °C/30 h in cross-section (TS: thermally sprayed coating; SM: substrate material) (a) bulk sample and (b) solution heat treated HVOF coating.

An increase in microhardness is caused by the phase transformation. The unaffected austenitic phase shows an average value of 334 HV 0.01, whereas the highest value was detected for the S-phase with a maximum at 1120 HV 0.01. No differences were observed depending on the distance to the surface. In accordance with this, the compound layer shows no gradient, whereas a slightly reduced microhardness was found. Table 5 summarizes the microhardness values of the different phases with their standard deviations.

Table 5. Microhardness of the different phases in the AISI 316L HVOF coating.

| Phase | Austenite | S-phase | Compound Layer |
|---------|-----------|----------|----------------|
| HV 0.01 | 334 ± 15 | 958 ± 86 | 861 ± 102 |

Depending on process parameters of the thermochemical treatment, a change in phase formation was observed by XRD studies, as shown in Figure 4. In comparison to the untreated sample, a shift of the characteristic peaks of the austenitic phase to lower angles was determined for the sample thermochemical treated at 420 °C. This can be explained by the increase of lattice spacing due to the interstitial inclusion of nitrogen atoms in the mixed crystal. Due to the different Young's moduli, the expansion of the lattice planes {111} and {200} differs. The lattice parameter of the austenitic phase extends from $a = 3.59 \text{ \AA}$ to $a = 3.92 \text{ \AA}$ for the planes {111}. Precipitates can be excluded for the

thermochemical treatment at 420 °C, but nitride phases occur at 520 °C. The characteristic peaks can be assigned to iron and chromium nitride phases.

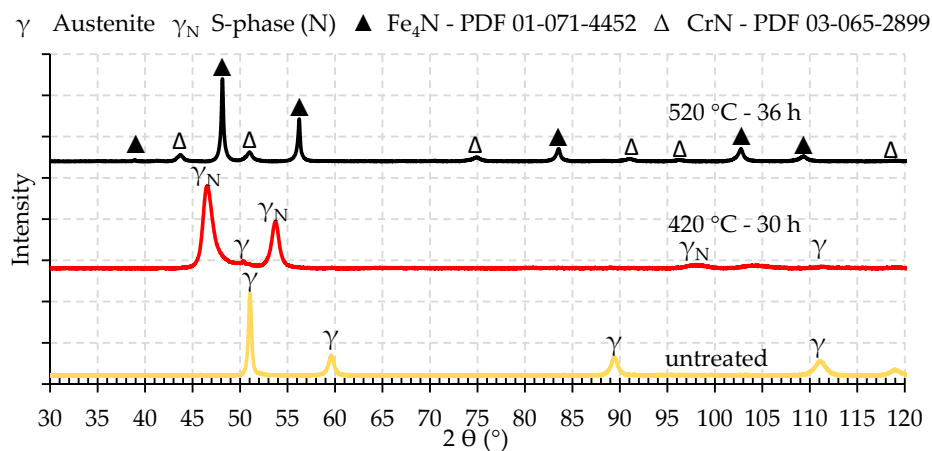


Figure 4. Diffraction diagrams of the gas nitrided and untreated AISI 316L HVOF coating in as-sprayed condition.

A significant increase in wear resistance of the coating was found for both gas-nitriding conditions, as shown in Figure 5. A reduction of the wear coefficient of more than 90% for sliding ball-on-disk test and approximately 75% for reciprocating ball-on-plane test was detected. As a consequence, the maximum values of wear depth were reduced in a similar manner.

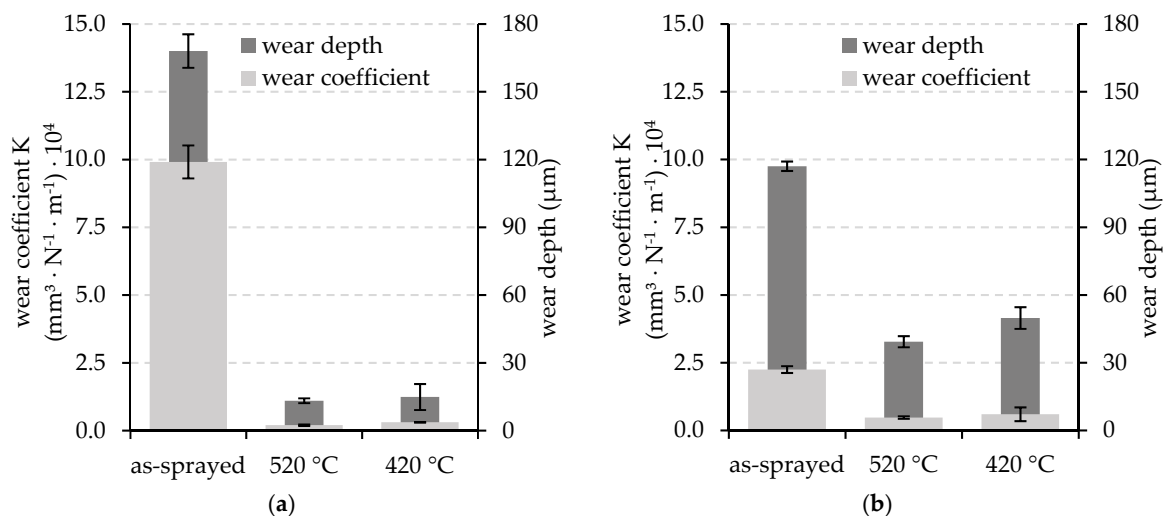


Figure 5. Wear values of the AISI 316L HVOF coating depending on the state of thermochemical treatment for different wear tests (a) ball-on-disk tests and (b) reciprocating ball-on-plane tests.

4. Summary

The results of the treatment of the coatings in as-sprayed condition prove that no additional activation step is required for successful diffusion enrichment by gas nitriding. This derives from the different material behaviors of bulk material and the coating. Phase formation depends on the temperature level and the duration time. Precipitation occurs under elevated temperatures, whereas the solid solution is supersaturated at a lower process temperature. A homogeneous precipitation layer grows from the coating's surface, whereas the S-phase is formed on the surface of the individual spray particles distributed between the surface and substrate. The coating's permeability allows for the penetration of gaseous enrichment media causing structural diffusion. A solution heat treatment of the coating reduces heterogeneity and a protective passive layer is formed. Solution and precipitation

hardening significantly improve the wear resistance. However, the differences between the various hardening mechanisms are minor, whereby S-phase formation prevents chromium depletion.

Author Contributions: T.L. (Thomas Lindner) and P.K. conceived and designed the experiments. T.L. (Thomas Lindner), P.K. and M.L. performed the experiments, analysed the data and wrote the paper. T.L. (Thomas Lampke) directed the research and contributed to the discussion and interpretation of the results.

Funding: This research received no external funding.

Acknowledgments: The authors thank Thomas Mehner for conducting the XRD measurements and Gunar Röllig for support in wear testing.

Conflicts of Interest: The authors declare no conflict of interest.

References

1. Somers, M.A.J.; Christiansen, T.L. Low temperature surface hardening of stainless steel. In *Thermochemical Surface Engineering of Steels*; Mittemeijer, E.J., Somers, M.A.J., Eds.; Elsevier Ltd.: Amsterdam, The Netherlands, 2015; pp. 557–579.
2. Zhao, C.; Li, C.X.; Dong, H.; Bell, T. Low temperature plasma nitrocarburising of AISI 316 austenitic stainless steel. *Surf. Coat. Technol.* **2005**, *191*, 195–200.
3. Bell, T. Current status of supersaturated surface engineered S-phase materials. *Key Eng. Mater.* **2008**, *373*, 289–295. [[CrossRef](#)]
4. Adachi, S.; Ueda, N. Combined plasma carburizing and nitriding of sprayed AISI 316L coating for improved wear resistance. *Surf. Coat. Technol.* **2014**, *259*, 44–49. [[CrossRef](#)]
5. Nestler, M.C.; Spies, H.; Hermann, K. Production of duplex coatings by thermal spraying and nitriding. *Surf. Eng.* **1996**, *12*, 299–302. [[CrossRef](#)]
6. Park, G.; Bae, G.; Moon, K.; Lee, C. Effect of plasma nitriding and nitrocarburizing on HVOF-sprayed stainless steel coatings. *J. Therm. Spray Technol.* **2013**, *22*, 1366–1373. [[CrossRef](#)]
7. Wielage, B.; Rupperecht, C.; Lindner, T.; Hunger, R. Surface modification of austenitic thermal spray coatings by low-temperature carburization. In Proceedings of the International Thermal Spray Conference & Exposition, Long Beach, CA, USA, 11–14 May 2015. DVS 276.
8. Adachi, S.; Ueda, N. Formation of S-phase layer on plasma sprayed AISI 316L stainless steel coating by plasma nitriding at low temperature. *Thin Solid Films* **2012**, *523*, 11–14. [[CrossRef](#)]
9. Adachi, S.; Ueda, N. Formation of expanded austenite on a cold-sprayed AISI 316L coating by low-temperature plasma nitriding. *J. Therm. Spray Technol.* **2015**, *24*, 1399–1407. [[CrossRef](#)]
10. Adachi, S.; Ueda, N. Surface hardness improvement of plasma-sprayed AISI 316L stainless steel coating by low-temperature plasma carburizing. *Adv. Powder Technol.* **2013**, *24*, 818–823. [[CrossRef](#)]
11. Lindner, T.; Mehner, T.; Lampke, T. Surface modification of austenitic thermal-spray coatings by low-temperature nitrocarburizing. *IOP Conf. Ser. Mater. Sci. Eng.* **2016**, *118*, 012008. [[CrossRef](#)]
12. Christiansen, T.L.; Hummelshøj, T.S.; Somers, M.A.J. Expanded austenite, crystallography and residual stress. *Surf. Eng.* **2010**, *26*, 242–247. [[CrossRef](#)]
13. Brink, B.K.; Ståhl, K.; Christiansen, T.L.; Oddershede, J. On the elusive crystal structure of expanded austenite. *Scr. Mater.* **2017**, *131*, 59–62. [[CrossRef](#)]
14. ASTM G 133 Standard Test Method for Linearly Reciprocating Ball-on-Flat Sliding Wear; ASTM International: West Conshohocken, PA, USA, 2016.
15. ASTM G 99 Standard Test Method for Wear Testing with a Pin-on-Disk Apparatus; ASTM International: West Conshohocken, PA, USA, 2016.
16. Rajendrana, P.; Devaraju, A. Experimental evaluation of mechanical and tribological behaviours of gas nitride treated AISI 316LN austenitic stainless steel. *Mater. Today Proc.* **2018**, *5*, 14333–14338. [[CrossRef](#)]
17. Subbiah, R.; Rajavel, R. Dry sliding wear behaviour analysis of nitrided 316LN grade austenitic stainless steels using gas nitriding process. *J. Theor. Appl. Inf. Technol.* **2010**, *19*, 98–101.

